A Sensor for the In-Flight Detection of Single Fluorescent Microbodies in Nanoliter Droplets

Michael Klinger, Christopher Laske, Mario Graeve, Martin Thoma, and Andreas Traube

***Abstract*—Single cell isolation is a crucial process step in many biological and pharmaceutical applications, as the number of technologies and assays for single cells is constantly rising. In this study, we propose a simple yet effective method for isolating single cells from a homogeneous solution. Therefore, we equip a high- throughput nano-dispenser system with a novel fluorescence-based in-flight cell detection sensor, which scans the dispensed droplets for the presence of a fluorescent cell on the fly. Based on initial studies on the dispensing physics, four different illumination and detection configurations of the sensor are presented and investigated. Finally, the system's performance in terms of detection rate, efficiency and process time is determined using cell-sized polystyrene microbeads as a reference standard. The results are very promising, as a 96-well plate is filled with single beads in under 60 seconds with a reproducible efficiency of more than 95%. Based on its generic design, the cell detection sensor is adaptable to virtually any low-volume dispenser, which is a major innovation over existing technologies.**

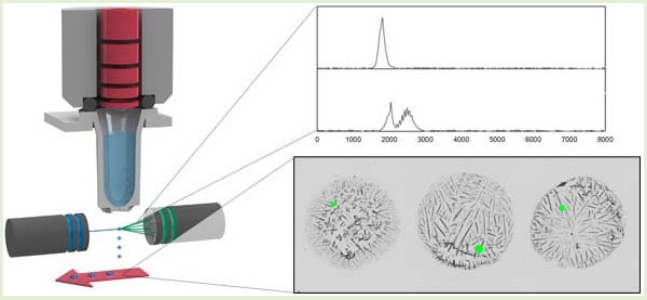

***Index Terms*— Single cell dispensing, fluorescent cell detection, sensor implementation.**

I. Introduction

THE isolation and deposition of single cells from a cell suspension is a key process step in various applications of biological and pharmaceutical research and production [1]–[3]. The differences of individual cells within a given population are potentially missed in traditional bulk analyses, which requires dedicated single cell analysis methods, such as next generation single cell sequencing, capable of the high-throughput transcriptomic analysis of individual cells [4], [5]. Another important application is the assurance of monoclonality in cell line development [6], where cells with desired characteristics for recombinant protein production need to be identified, isolated and then cultivated for improved antibody production [7], [8].

The increasing availability of single cell technologies has led to a growing demand for isolation and deposition techniques [9]–[11]. Depending on the actual application, the key parameters of such systems are throughput, efficiency (i.e. the percentage of actual single cells, in relation to the total number of target containers) and impact on cell viability and cell functionality (proliferation).

According to Gross *et al.* [9], the most commonly utilized techniques for non-manual single cell isolation are FACS (fluorescence activated cell sorting) and limiting dilution (also referred to as "random seeding"). In FACS, the cell suspension is pumped through a microfluidic channel at high speed, where the fluorescent cells are excited by a LASER and detected by PMTs (photomultiplier tubes). Subsequently, the cells exit the microfluidic channel, thereby crossing a controllable electric field, which deflects selected droplets into target containers, enabling the sorting and / or isolation of the cells. The approach of limiting dilution on the other hand, is much simpler: The cell suspension with a given cell concentration is dispensed into the desired target containers at a fixed volume, such that the probability of the fixed volume containing exactly one cell maximizes.

Whereas limiting dilution is fast, simple, cost-effective and can be implemented on virtually any dispensing system, it lacks single cell efficiency. The underlying principle of the Poisson distribution limits the theoretical maximum efficiency of about 37 % [12], leaving the rest of the target containers empty, or filled with more than one cell. FACS in comparison, is very fast and efficient, however existing systems are costly and non-negligible impact on cell viability has been reported [13]. Over the past years, a couple of new approaches

Manuscript received March 25, 2019; revised September 3, 2019 and February 3, 2020; accepted February 4, 2020. Date of publication February 7, 2020; date of current version May 5, 2020. This work was supported by the Fraunhofer-Gesellschaft zur Förderung der angewandten Forschung e.V. The associate editor coordinating the review of this article and approving it for publication was Dr. Shyqyri Haxha. *(Corresponding author: Michael Klinger.)*

Michael Klinger, Mario Graeve, Martin Thoma, and Andreas Traube are with the Fraunhofer Institute for Manufacturing Engineering and Automation IPA, 70569 Stuttgart, Germany (e-mail: michael.klinger@ipa.fraunhofer.de).

Christopher Laske is with Dispendix GmbH, 70569 Stuttgart, Germany (e-mail: christopher.laske@dispendix.com).

Digital Object Identifier 10.1109/JSEN.2020.2972268

were presented, which claim to fill the gap between the simple limiting dilution and the sophisticated FACS method. Most of them feature pre- or post-dispense imaging solutions, such as [14] or [15].

II. Concept and System Overview

The overall objective of this work is the development of a single cell isolation technique that combines the positive aspects of all the presented solutions available today. The basic idea is to implement limiting dilution on a high-throughput nano-dispensing system and enhance its efficiency through a real-time in-flight cell detection system.

Since cell dispensing is a very complex and multi-faceted undertaking, that requires comprehensive studies on different cell types, cell media and fluorescent stains, we decided to step into the development process with a more general approach. For that reason, we investigated the feasibility of detecting fluorescent microbodies within falling nanoliter droplets, which represents a more general abstraction of the cell detection problem.

In the following paragraphs, we will present the working principle of the cell isolation procedure, the utilized components for the dispenser and the sensor as well as the related physical challenges.

A. Cell Isolation Procedure

The isolation of single cells is achieved by dispensing droplets of a relatively low cell concentration, while simultaneously detecting fluorescent cells therein. The dispensing process runs until the cell detection sensor registers a cell in a droplet. In that case, the process is paused immediately and then resumed with a new target container. As a result, every addressed target container should contain at least one cell.

The underlying stochastic process is defined by the Poisson distribution, which describes the probability of occurrence for discrete and independent events. It is widely used to express probabilities for single cell dispensing, especially in limiting dilution applications [16], [17].

Equation (1) describes the Poisson probability $P_\lambda(k)$ for a natural number k (cell count) and a given expected value λ, defined by the droplet volume $V_{Droplet}$ and the initial cell concentration C (2).

$$P_\lambda(k) = \frac{\lambda^k}{k!} e^{-\lambda} \tag{1}$$

For a droplet volume of 10 nl, and a cell concentration of 0.2 cells / nl, for example, λ computes to 2.0, which means that every droplet contains two cells on average.

$$\lambda = \frac{V_{Droplet}}{C} \tag{2}$$

When equipped with a cell detection sensor, the system is supposed to dispense mostly empty droplets (since we are using a low cell concentration, $\lambda < 1.0$) until one or more cells are registered by the sensor. In that case, we need to compare the probability of ending up with one cell in the droplet compared to two or more cells. Thus the probability of depositing exactly one cell $P_{Single}(\lambda)$ can be evaluated to:

$$P_{Single}(\lambda) = \frac{P_\lambda(1)}{\sum_{n=1}^{\infty} P_\lambda(n)} = \frac{P_\lambda(1)}{1 - P_\lambda(0)} \tag{3}$$

The final single cell efficiency (number of targeted wells containing exactly one cell in relation to the total number of targeted wells) therefore solely depends on the initial cell concentration, which affects the probability of enclosing two or more cells within a single droplet (3). Fig. 1 shows the calculated efficiencies for different λ-values. A value of $\lambda = 0.01$ for example, leads to an expected efficiency of about 99%, however an average of 100 droplets per cell needs to be dispensed, which negatively affects the throughput of the system.

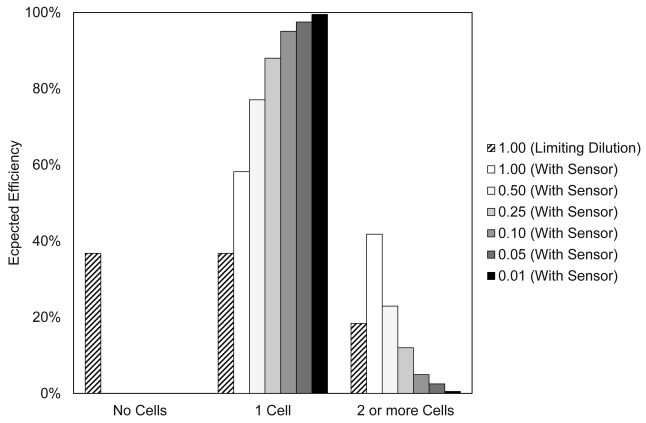

Fig. 1. Theoretical single cell efficiencies for different expected values λ, ranging from 1.0 “P” (normal Poisson distribution) over 1.0 “S” (with Sensor) to 0.01 “S” (right).

B. The Immediate Drop on Demand Technology

For the generation of the droplets, we incorporate the immediate drop-on-demand technology (I-DOT) [18], [19]. The working principle of the dispenser is based on the application of short pressure pulses onto the surface of a liquid, located in a modified well of microwell plate. The wells have a small nozzle at their bottom (60 μm or 90 μm in diameter, depending on the addressed droplet volume range), which is small enough to retain the liquid in the well under normal conditions (surface tension). For each pressure pulse applied to the liquid, the pressure in the well rises shortly and a small droplet is ejected through the nozzle at the bottom (see Fig. 2).

The fabrication of the source wells is a two-step process: First, a through hole with the respective nozzle diameter is etched into the center of a square silica chip with 2 mm × 2 mm and a thickness of 300 μm. This procedure allows maximum precision in the nozzle diameter. Subsequently, the walls of the well are casted around the chip by injection molding. The resulting container has an inner volume of about 80 μl.

The presented dispensing principle is particularly suitable for the purpose of this study for various reasons:

- The form and volume of the droplets can be easily adjusted from spherical droplets (minimum 2 nl, utilizing

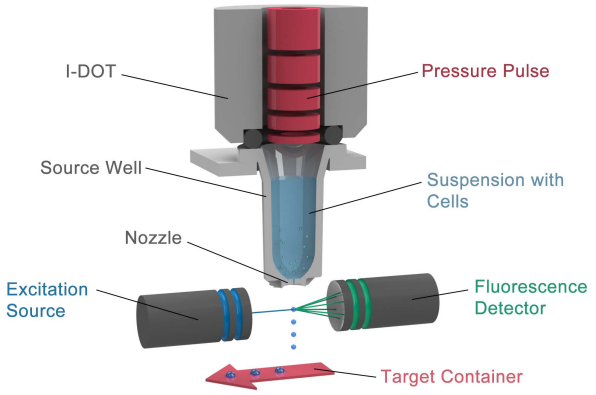

Fig. 2. The principle of the I-DOT dispensing system equipped with a fluorescence-based cell detection. Media with fluorescent microbodies is filled into the source well. The nozzle (60 μm diameter) is small enough to retain the liquid in the well (surface tension). The I-DOT-Device applies short pressure pulses on the surface of the liquid, which leads to the ejection of small droplets from the bottom of the nozzle towards the target container (illustrated as red arrow). The droplets are scanned for the presence of a fluorescent microbody through the proposed sensor on the fly.

the 60 μm nozzle) up to larger droplets, so called jets (maximum 40 nl, utilizing the 90 μm nozzle) by adjusting the so called "dosing energy" [19], which we will explain later on.

- The dispensing principle is well suited for cell dispensing in general. The method of the droplet generation does not have any significant impact on cell viability and / or cell proliferation and functionality, as previous studies have shown [20].
- The dispensing rate of up to 400 droplets per second [19] offers high potential for fast and efficient single cell deposition.
- The technology is an in-house development and therefore provides open interfaces for integration and adaption, which simplifies the development of an attached cell sensor system.

C. Dispensing Physics

The physics behind the droplet formation process, based on the fluid flow through a small nozzle has been intensively studied in [21] and [22], and is not subject to this investigation. The geometric shape of the resulting droplet and its volume are yet important parameters for the detection of (single) microbodies therein.

The dosing energy E_d applied to the source well has a near-linear correlation with the resulting droplet volume and can be controlled continuously through the I-DOT-Software. It is defined as the integral of the pressure pulse over time, measured in the middle between the actuating fast switching valve, and the liquid surface of the source well. The pressure P on the input side of the valve has a constant value of $200,000\,Pa = 2\,bar$.

$$E_d = \int P\,(t)\,dt \tag{4}$$

Within the I-DOT ecosystem, the dosing energy's basic unit is described as Laske (La) [19].

$$[E_d] = 1La = 1mbar * 1ms \tag{5}$$

TABLE I
RELATIONSHIP BETWEEN DOSING ENERGY, THE RESULTING DROPLET VOLUME AND ITS VELOCITY. THE LATTER WAS OBSERVED FROM THE IMAGES IN FIG. 2 (VALID FOR WATER-BASED LIQUIDS, SUCH AS PBS AND VARIOUS CELL MEDIA, DISPENSED WITH A 60 μm NOZZLE)

Dosing Energy E_d	Average Droplet Volume V_d	Droplet Front-Velocity v_d
75 La	3 nl	0.70 m/s
100 La	4 nl	1.49 m/s
150 La	6 nl	2.67 m/s
200 La	8 nl	3.62 m/s
250 La	10 nl	4.69 m/s
300 La	12 nl	5.93 m/s

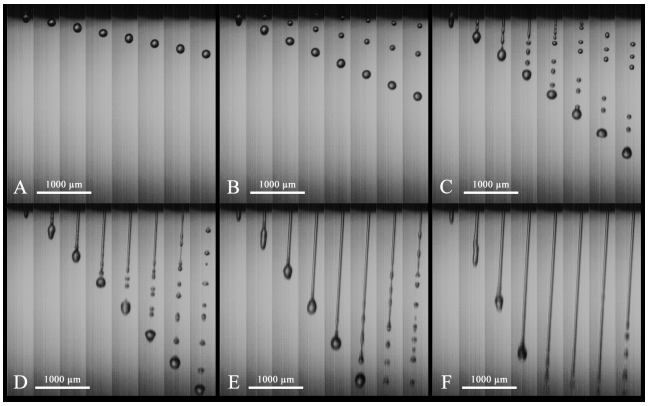

Fig. 3. High speed image sequences of the droplet formation process of water for different dosing energies, captured at a fixed rate of 7,600 frames per second and an integration time of 20 μs. (A) dosing energy = 75 La, (B) dosing energy = 100 La, (C) dosing energy = 150 La, (D) dosing energy = 200 La, (E) dosing energy = 250 La, (F) dosing energy = 300 La.

For the correlation of volume and geometric shape of the droplet, a series of high-speed images of the droplet formation process of water has been captured for different dosing energies and a fixed nozzle diameter of 60 μm (Fig. 3). For a given liquid class (a subset of liquids with similar physical properties, leading to a similar dosing results), the linear approximation function between dosing energy and droplet volume can be determined as described by Kroll [23] and Holz-Müller [24]. Table I shows the relationship for water-based liquids, as well as the resulting droplet velocities, observed from the images in Fig.3.

The lowest dosing energy, at which water droplets can be reproducibly generated is about 75 La. The impact of the liquid's surface tension and the relatively low kinetic energy causes the water to form a round sphere after it becomes detached from the nozzle. When the dosing energy is increased to 100 La, a bigger volume is pressed through the nozzle, forming a very short liquid jet that immediately breaks apart into separate round droplets. Increasing the dosing energy further on, the jets become longer, faster and especially more stable, even though the end part of the jet will always collapse into droplets. This effect has been observed for water-based

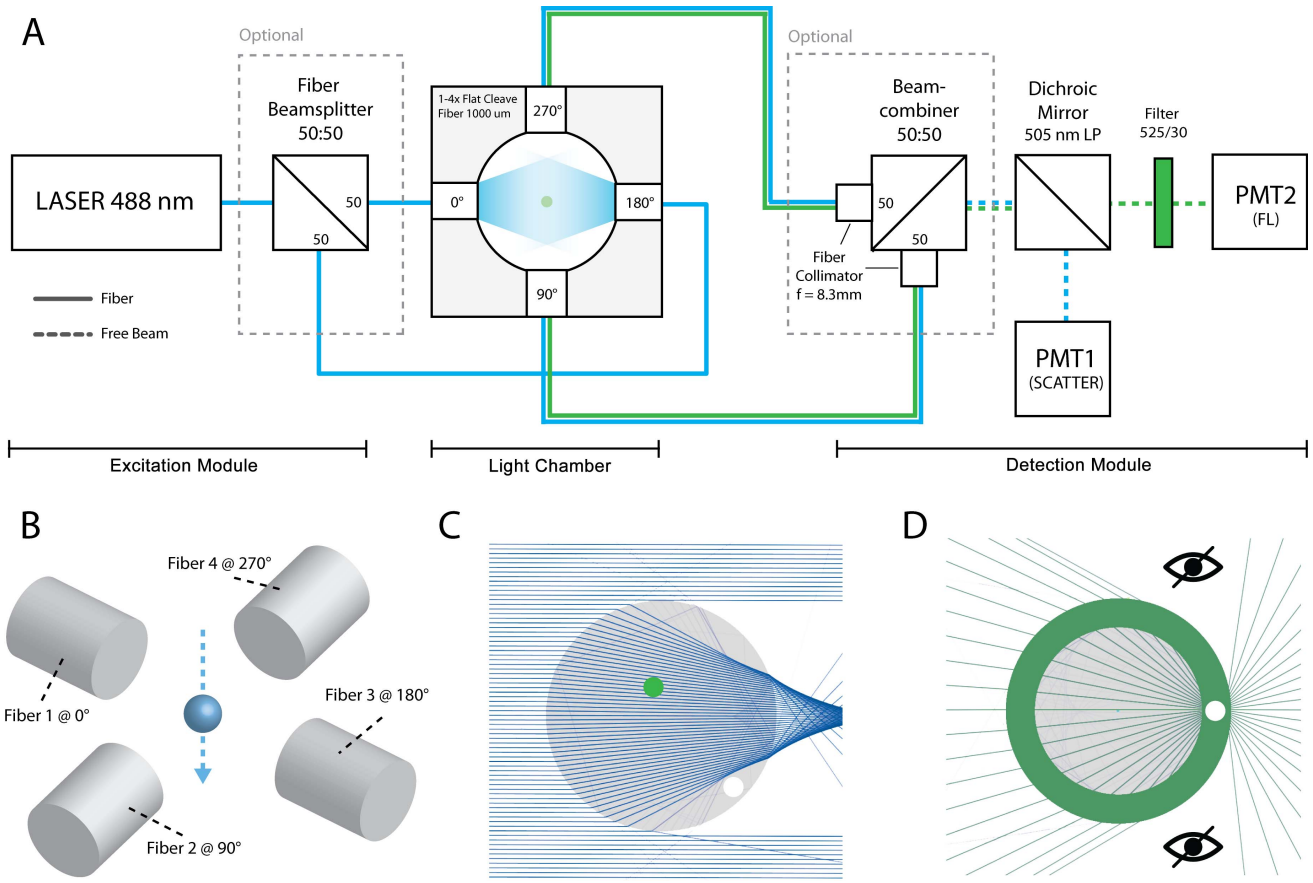

Fig. 4. (A) Schematics of the optical sensor arrangement, incorporating a LASER module, connected to a variable light chamber (B) via optical fiber cables, and a detection module, which enables the acquisition of scattered light and fluorescence light via photomultiplier-tubes. The variable light chamber (B) offers four fiber ports, arranged in 90° angles in the plane perpendicular to the axis of the falling droplet, which might be connected to either the LASER or the detection module. (C) An abstraction of the illumination problem: Parallel incident light (coming from the left) does not illuminate all parts of the droplet homogeneously, causing cells in the center to be excited, whereas cells in the right border region are not excited (D) An abstraction of the observation problem: When a cell is located in the border region of the droplet, a portion of the light is able to leave the droplet, the rest is "trapped" due to total internal reflection, causing observers outside the droplet to miss the cell.

liquids and can only be mitigated by liquids with a smaller Weber-number [21].

D. Sensor Design

Due to the fact that liquid droplets ejected from the nozzle do not necessarily travel in a perpendicular manner, the target carrier - usually a microwell plate (MWP) containing multiple target containers - should preferably be positioned as close as possible to the source well, in order to avoid inclining droplets to miss the target. This circumstance does not allow the installation of larger optical components close to the nozzle. Instead, a solution incorporating optical fiber cables is chosen, allowing a remote installation of excitation and detection optics. Based on the assumption, that the position and orientation of light source(s) and detector(s) will affect the detection rate, multiple setups will be investigated. Fig. 4 shows a macroscopic scheme of the optical sensor design, as well as the different fiber setups.

Since there is a vast number of different established staining and protein expression mechanisms for cell fluorescence that work on different wavelengths, the system needs to be designed for a specific fluorochrome. Based on its popularity in the biochemical and cellular research, Fluorescein is chosen due to its versatility and availability [25]. The peak excitation wavelength of Fluorescein is about 494 nm and the peak emission wavelength is about 520 nm.

For the excitation of the microbodies, we use a fiber-coupled multimode LASER module from Coherent (BioRay FR, Santa Clara, USA), with a typical wavelength of 488 nm and a maximum output power of 120 mW. All other optical components were purchased from Thorlabs (Newton, USA). The fibers that connect the LASER respectively the detection module to the light chamber (see Fig. 4) have an internal diameter of 1000 μm, and a numerical aperture of 0.50. The four fiber ports are arranged in 90° angels in the plane perpendicular to the axis of the falling droplet with a displacement of 2.5 mm to the axis. All fiber ends pointing towards the droplet have a flat cleave.

In the detection module (see Fig. 4), the incoming light is directed to a dichroic long pass mirror (505 nm) which splits the light into two separate paths, allowing the parallel detection of scattered excitation light and fluorescence light of the microbodies through photomultiplier modules (PMT1, PMT2) (both PMM02, Thorlabs, Newton, USA). The latter is equipped with an additional bandpass filter with a center

wavelength of 525 nm and a bandwidth of 30 nm. For those setups, where two fibers need to be connected to the LASER, respectively the detection module, 50:50 beamsplitters were inserted into the light paths (as illustrated in Fig. 4).

E. Sensor Integration

The light chamber is integrated into the base plate of the I-DOT, which also secures the source well during dispensing. The fibers are located directly underneath the well, such that the maximum excitation of the droplets will occur about 1.5 mm beneath the nozzle. The PMTs are controlled through a specifically designed electrical circuit hosting a STM32F4 microcontroller (ST Microelectronics, Amsterdam, Netherlands) as main computing element. When the I-DOT system generates a droplet, the controller triggers the acquisition of the analog output voltage of the PMTs through the integrated analog to digital converter. The acquisition length is limited to 8 ms for each droplet, whereas the actual signal peak is expected to show at about 1.5 ms to 5 ms after the valve opens, depending on the dosing energy applied. Subsequently, the signals are transferred to a PC-Software through the serial port for further evaluation and analysis. The static offset (caused by minimal stray light) is subtracted from each signal. No additional filtering is applied.

F. Implications for the Cell Detection

The boundary between two media with different refractive indices causes light to refract and / or reflect. If the light is not incident perpendicular to the boundary, the apparent location of the object is different from the actual position of the object. In many applications where cells or other small particles are being observed, e.g. microscopy or flow cytometry, it is desired to have a nearly perpendicular angle of light incidence towards the transition surface (e.g. a flat glass slide or a rectangular flow channel), in order to avoid these phenomena.

Surface tension causes water to coalesce into near spheres. Upon interaction with light, a curved refractive index boundary is inevitable. As a first approximation, the droplets can be described as objects that are rotationally symmetrical to the motion axis, so we can conceive the impact of the geometry on the ability to illuminate and observe the cell within the droplet. Fig. 4C illustrates the incoming and outgoing ray paths for external illumination. The droplet acts as a collimating lens. Irrespective of the direction of illumination, some regions of the drop remain dark (hereinafter referred to as "blind" regions). Fig. 4D illustrates the inverse problem, a point light source (e.g. a fluorescent cell) located at the very border, but inside the droplet. The emerging ray paths from the droplet do not allow the formation of an image. In some regions, outside observers will not register any light emitted from the cell. The majority is "trapped" due to total internal reflection.

The idea of the "variable light chamber" proposed in Fig. 2 is that simultaneous illumination and observation from multiple angles helps to negate these effects.

III. Experimental Results

In this section, we will present experimental results that were achieved with the proposed cell detection and isolation system. In order to generate reproducible and quantifiable results, we utilize cell-sized polystyrene microbeads "Fluoresbrite® YG Microspheres" (Polysciences, Warrington, USA), which come with a pre-stained fluorescent surface similar to Fluorescein. The beads have an average diameter of 6 μm and are highly uniform in size and fluorescent intensity. Their excitation maximum is located at 441 nm and the emission maximum is located at 486 nm [26], however due to their broad spectral range, they can be easily detected with the proposed optical system.

In comparison to stained cells, or cells that express a fluorescent protein, the beads are typically more homogeneous, are easier to handle and most importantly more stable over time. These features qualify the beads as an ideal reference-model for the evaluation of the system.

For all experiments, the beads were diluted in phosphate buffered saline (PBS) in order to retrieve the empty droplets under the microscope. In contrast to water droplets, the evaporated PBS-droplets leave an easy-to-detect pattern of saline crystals (see Fig. 6).

A. Comparison of Light Setups

In order to measure the impact of different illumination and detection setups, we dispense single droplets and jets onto microscope glass slides and evaluate their content with the fluorescence imager Cytation 5 (BioTek, Winooski, USA) later on (see Fig. 6). The following four optical setups were investigated, with a total number of 768 dispensed droplets / jets each (see Fig. 5).

Steup 1) Excitation from fiber 1 (0°), detection from fiber 2 (90°). Fiber 3 and 4 are disconnected.

Steup 2) Excitation from fiber 1 (0°), detection from fiber 2 (90°) and fiber 4 (270°). Fiber 3 is disconnected.

Steup 3) Excitation from fiber 1 (0°) and fiber 3 (180°), detection from fiber 2 (90°). Fiber 4 is disconnected.

Steup 4) Excitation from fiber 1 (0°) and fiber 3 (180°), detection from fiber 2 (90°) and fiber 4 (270°)

Since the actual amount of single beads dispensed onto the slides depends on the initial bead concentration, we optimized the concentrations for droplets and jets in order to achieve a λ-value of about 1.0 (which maximizes the single bead probability to about 37% in theory). For each dispensed droplet / jet, we acquired the fluorescence signal of the PMT (2) in order to correlate it with the content of the respective droplet afterwards (number of beads found in the microscopic image of the evaporated droplet).

Fig. 5 shows histograms of the relative frequency of the measured peak fluorescence signal voltages in all droplets that were identified as containing exactly one bead. Droplets that contained more than one bead were not considered in this evaluation. Empty droplets were not showing any significant fluorescence signal and had peak values of less than 250 mV above the baseline, caused by stray light and electrical noise from the PMT and its integrated transimpedance amplifier.

Comparing the histograms in Fig. 5, the peak signal voltages for jets show less variation than the signals for droplets,

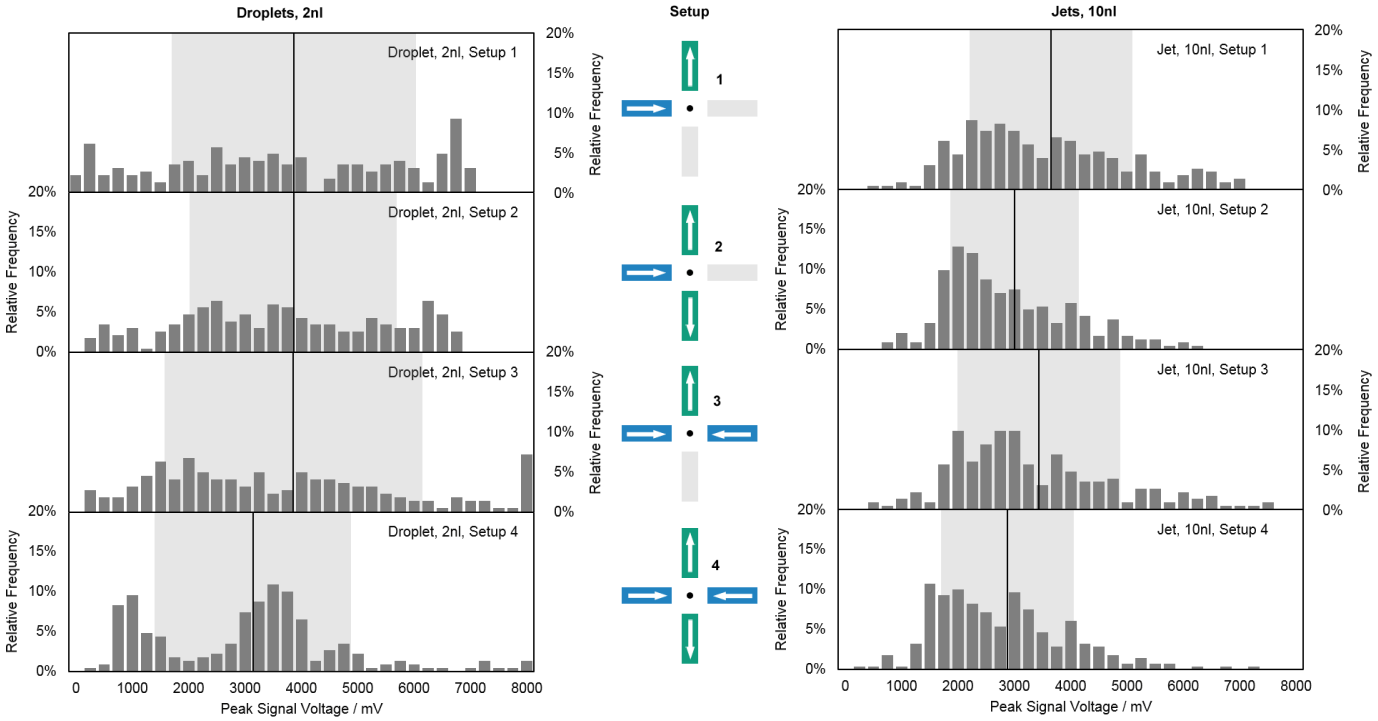

Fig. 5. Signal histograms for different light setups (1-4) and different geometries / volumes (2 nl droplets, 10 nl jets). The histograms show the relative frequency of the peak fluorescence signal (in mV) in all droplets that were identified as containing exactly one bead. Vertical black lines indicate average values, gray boxes indicate region of standard deviation (2σ). The number of data points varies due to the unpredictable number of dispensed single beads and ranges between 222 and 280 points per histogram, which correlates to single bead efficiencies between 28.9 % and 36.4 %.

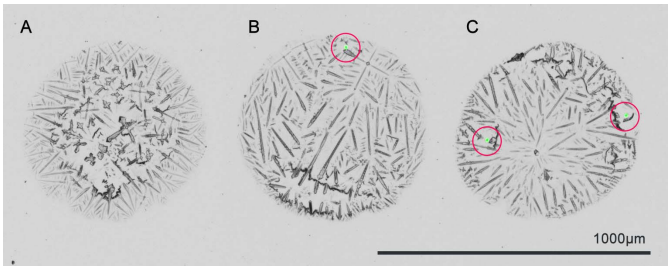

Fig. 6. Microscopic images of the evaporated droplets (10 nl jets) on the glass slide, consisting of one brightfield exposure and one blended fluorescence exposure. Beads are green and are marked with a red circle. The droplets contain no (A), one (B), and two (C) beads.

irrespectively from the chosen light setup. This observation can be related to the fact that the droplet geometry works as a collimating lens, focusing incoming light towards the center and thus creates very bright regions (where beads are excessively excited), whereas regions at the border remain dim (where beads are excited only moderately or not at all). Adding additional light sources and detectors helps to improve this circumstance, however the top and bottom part of the droplet is still affected. The data from the jets shows less variation, suggesting a more homogeneous illumination.

Comparing the different light setups for the droplets, the average peak signals as well as their standard deviation do not change significantly. However, the additional light sources and detectors (setup 2 – 4) help to decrease the number of low signals ($V < 500$ mV), which positively affects the detection rate (the system's ability to correctly discriminate between empty and non-empty droplets): Setup 4 has produced only one signal with a peak of less than 500 mV.

For the larger jets, the differences between the setups are even smaller. However, the introduction of a second detector leads to an increase in homogeneity (smaller standard deviation) as the data for setup 2 and 4 indicates. On the other hand, the average peak signal is slightly decreased. These observations apply to the smaller droplets as well.

Conclusively, the data clearly states that the cell detection will work better for larger volumes, based on their geometric and thus optical properties of the droplet. When smaller droplet volumes are desired, the introduction of a second detector and a second illumination source will noticeably improve the signal strength in the lower regions. This is particularly useful when real cells are dispensed, since their fluorescence emission (either staining or protein expression) is generally less intense and also less uniform, based on the higher inhomogeneity in their size.

B. Bead Count Analysis

As a next step, we investigate the system's ability to discriminate between droplets containing exactly one bead and droplets that contain multiple beads. For this purpose, we revise the signals acquired in the previous experiment, however we consider the empty and multi-bead droplets as well. Based on the results from the previous experiment,

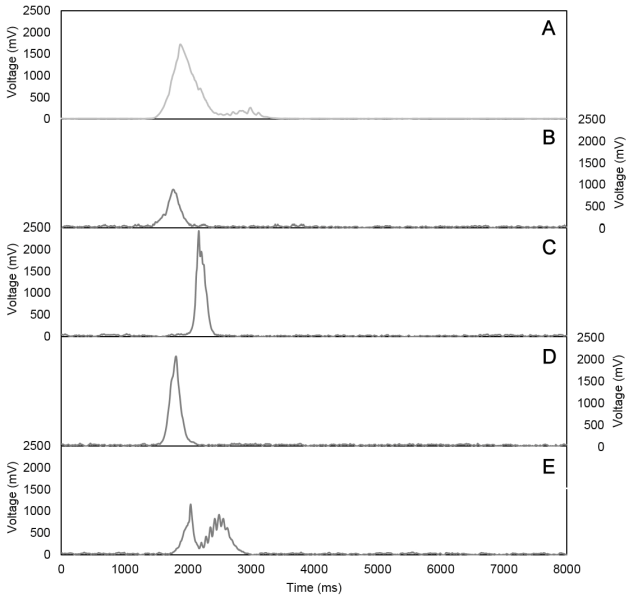

Fig. 7. Signals acquired by the detection system: A) shows a representative scatter signal of a 10 nl jet B) and C) show fluorescence signals of single beads within a jet, exhibiting different signal intensities and timings. D) and E) show fluorescence signals of jets containing two beads, where in D) the beads seem to be close together, resulting a in superposition of signal peaks and in E), the signals have a slight time offset, suggesting a different position within the jet.

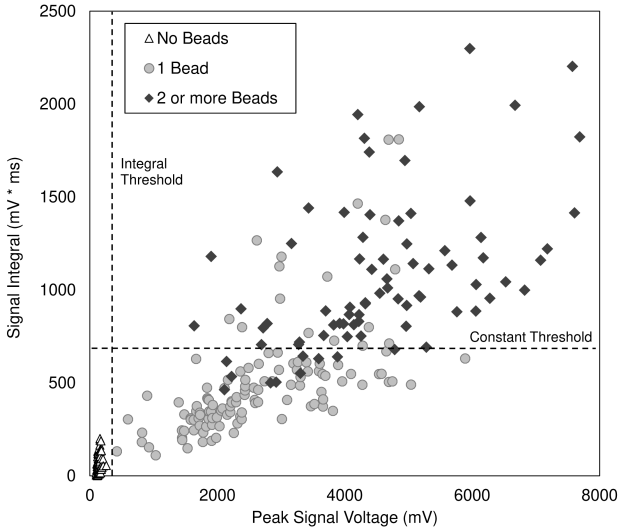

Fig. 8. Scatter plot of fluorescence signals from 10 nl jets, processed in setup 4. The x-axis shows the peak signal in mV, the y-axis shows the integral signal value in (mV * ms). The vertical dashed line indicates the proposed threshold for the discrimination between empty and non-empty droplets, the horizontal dashed line indicates the proposed threshold for the discrimination between droplets containing one and two or more beads.

we continue with setup 4 and dispense jets with 10 nl volume, as this combination showed the best performance.

The chances of detecting two beads in a droplet using the signal intensity is very low, given the non-uniform distribution of peak signals. An example of such non-uniform single bead signals can be obtained from Fig. 7b and Fig. 7c, as both signals represent a droplet containing one bead only. Furthermore, the signal from Fig. 7d is comparably high as the one from Fig. 7c, however the related droplet contained two beads. Depending on the beads' position within the droplet, it can also occur that the individual peaks have a slight delay in time (as in Fig. 7e), which simplifies the quantification of beads in the droplet. It is assumed that the individual beads create a signal according to the histogram distribution described in the previous section, and are simply superimposed onto the resulting signal.

In order to investigate the feasibility of discriminating between the signals, we plotted the peak signal voltage as well as the signal integral for each droplet into a scatter plot (see Fig. 8). The discrimination between empty droplets and droplets containing beads can easily be achieved by a constant threshold algorithm, since the peak signal voltages differ noticeably. With a threshold of 300 mV, a 100 % detection rate can be achieved (based on the data of the 768 jets). For the differentiation between signals of droplets containing one and two or more beads, neither the peak signal voltage, nor the signal integral can guarantee an error-free detection. However for the presented set of data, the signal integral is the better choice of both, leading to an 87 % success rate, when a threshold of 680 mV∗ms is assessed. The success rate in this case, is the percentage of non-empty droplets that have correctly been assessed as containing one or more than one bead by the algorithm.

For the proposed single cell isolation procedure, the discrimination between empty and non-empty droplets is essential, as it directly affects the efficiency of the system. The discrimination between one and two or more beads however is not as crucial, as a successful analysis will not prevent the droplet with multiple beads from falling into the target, negatively affecting the efficiency. Instead, the information can only be used to mark the respective target, if this is desired for the downstream process.

C. Single Bead Isolation

As a last experiment, the systems primary purpose – single cell isolation – is tested. Again, the beads were dissolved in PBS at different concentrations, ranging from 64,000 beads / ml down to 4,000 beads / ml (5 concentrations in total), which correlates to λ-values of 0.64 down to 0.04 for a given fixed droplet volume of 10 nl. As target container, standard 96-well plates with a prefilled PBS-volume of 100 μl per well were used. Each concentration was utilized four times, to fill all wells of a plate with single beads (288 wells per concentration). The dispensing rate was set to 100 droplets per second, whereas the system immediately pauses the processes upon the registration of a signal (300mV threshold), addresses a new target container and then resumes the dispensing. Again, optical setup 4 was utilized for best performance.

Afterwards, the wells were imaged with the Cytation 5 imager system and the number of beads per well was recorded. Fig. 8 shows the determined single bead efficiency per concentration (percentage of wells containing exactly one bead).

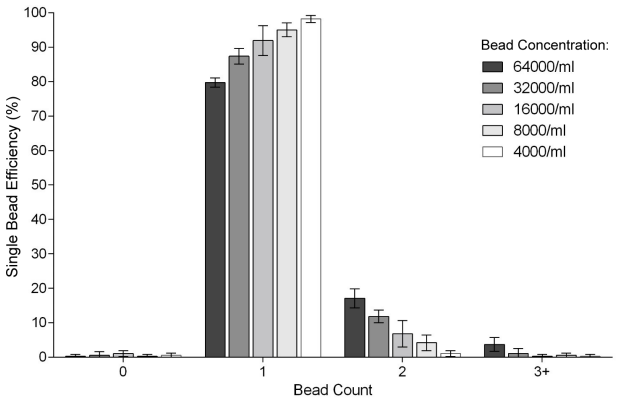

Fig. 9. Single bead efficiency for various cell concentrations and a droplet volume of 10 nl. The whiskers indicate the standard deviation between the results of each individual plate (n=4).

The total number of empty wells was very low (< 1.5 %) throughout all concentrations, showing the robustness of the threshold detection. The percentage of single beads is increasing with each dilution step of the cell concentration, following the logic of the Poisson distribution explained in Chapter II. For optimal performance, the system is able to reach a single bead efficiency of 98 % with a concentration of 4,000 beads / ml, which correlates to one faulty well per plate.

However, the reported efficiency numbers do not quiet reach the theoretically conceivable numbers, which is possibly caused by various reasons: The bead solution is not absolutely homogeneous, the dispensed droplet volume has an average coefficient of variation of about 3 % [19], and some beads are potentially missed in the imaging step, as they stick to the wall of the well or do not sediment into the focal plane at all.

The process time of one 96-well plate depends on the bead concentration, since more droplets need to be dispensed for the lower concentrations. An average time of 47 s was recorded for 64,000 beads / ml and 61 s for 4,000 beads / ml.

IV. Conclusion

The presented sensor design is capable of detecting microscopic fluorescent particles in nanoliter PBS-droplets very reliably. The acquisition of high speed images of the droplet formation process has helped to understand the underlying physics and emphasized the results of the different illumination and detection setups. A combination of multiple detectors and one - better two - light sources has improved the signal homogeneity and thus the detection rate and feasibility of the bead count analysis.

For the optimal setup (4), the detection rate of beads was 100 % in a total set of 768 dispensed droplets, using a simple voltage threshold. With an additional threshold for the signal's integral value, the differentiation between one and two or more beads per droplet was successful in 87% of all cases.

The resulting single bead efficiency for low concentrations of about 98% for 4,000 beads / ml is very promising, as it is comparable to well established technologies available on the market. However, the achieved throughput of one 96-well plate per minute is currently unreached, and makes the system particularly suitable for high-throughput applications.

Another advantage of the presented cell detection sensor is its generic design, which allows the integration into virtually any low-volume dispenser.

V. Outlook

It was demonstrated, that the proposed sensor system performed very well with the utilized polystyrene microbeads, as they are an ideal reference standard for fluorescence cell applications. Since the system is actually designed to dispense living cells, additional experiments have to show the proof of principle for cells as well. Besides a less intense and less uniform staining, which will be an additional challenge for the detection sensor, the system's impact on the cell viability and cell proliferation must be investigated properly. Furthermore, commonly used cell media has additional ingredients, such as buffer substances, nutrients and serum, which may negatively affect the dispensing physics, as the viscosity is increased.

References

[1] S.-B. Liang and L.-W. Fu, "Application of single-cell technology in cancer research," *Biotechnol. Adv.*, vol. 35, no. 4, pp. 443–449, Jul. 2017.
[2] P. Hu, W. Zhang, H. Xin, and G. Deng, "Single cell isolation and analysis," *Frontiers cell Developmental Biol.*, vol. 4, p. 116, Oct. 2016.
[3] S. Ishii, K. Tago, and K. Senoo, "Single-cell analysis and isolation for microbiology and biotechnology: Methods and applications," *Appl. Microbiol. Biotechnol.*, vol. 86, no. 5, pp. 1281–1292, May 2010.
[4] A. Kolodziejczyk, J. K. Kim, V. Svensson, J. Marioni, and S. Teichmann, "The technology and biology of single-cell RNA sequencing," *Mol. Cell*, vol. 58, no. 4, pp. 610–620, May 2015.
[5] D. Wang and S. Bodovitz, "Single cell analysis: The new frontier in 'OMICS,'" *Trends Biotechnol.*, vol. 28, no. 6, pp. 281–290, 2010.
[6] K. Evans *et al.*, "Assurance of monoclonality in one round of cloning through cell sorting for single cell deposition coupled with high resolution cell imaging," *Biotechnol. Prog.*, vol. 31, no. 5, pp. 1172–1178, Sep. 2015.
[7] H. Le, N. Vishwanathan, N. M. Jacob, M. Gadgil, and W.-S. Hu, "Cell line development for biomanufacturing processes: Recent advances and an outlook," *Biotechnol. Lett.*, vol. 37, no. 8, pp. 1553–1564, Aug. 2015.
[8] J. Fieder, P. Schulz, I. Gorr, H. Bradl, and T. Wenger, "A single-step FACS sorting strategy in conjunction with fluorescent vital dye imaging efficiently assures clonality of biopharmaceutical production cell lines," *Biotechnol. J.*, vol. 12, no. 6, Jun. 2017, Art. no. 1700002.
[9] A. Gross, J. Schoendube, S. Zimmermann, M. Steeb, R. Zengerle, and P. Koltay, "Technologies for single-cell isolation," *Int. J. Mol. Sci.*, vol. 16, no. 8, pp. 16897–16919, Jul. 2015.
[10] C. W. Shields, K. A. Ohiri, L. M. Szott, and G. P. López, "Translating microfluidics: Cell separation technologies and their barriers to commercialization," *Cytometry*, vol. 92, no. 2, pp. 115–125, Mar. 2017.
[11] Y. Wang and N. Navin, "Advances and applications of single-cell sequencing technologies," *Mol. Cell*, vol. 58, no. 4, pp. 598–609, May 2015.
[12] R. Staszewski, "Cloning by limiting dilution: An improved estimate that an interesting culture is monoclonal," *Yale J. Biol. Medicines*, vol. 57, pp. 865–868, Nov. 1984.
[13] M. Mollet, R. Godoy-Silva, C. Berdugo, and J. J. Chalmers, "Computer simulations of the energy dissipation rate in a fluorescence-activated cell sorter: Implications to cells," *Biotechnol. Bioeng.*, vol. 100, no. 2, pp. 260–272, Jun. 2008.
[14] A. Gross *et al.*, "Single-cell printer: Automated, on demand, and label free," *J. Lab. Automat.* ., vol. 18, no. 6, pp. 504–518, Dec. 2013.
[15] A. Yusof *et al.*, "Inkjet-like printing of single-cells," *Lab Chip*, vol. 11, no. 14, pp. 2447–2454, 2011.
[16] J. Quiroz and Y.-S. Tsao, "Statistical analysis of data from limiting dilution cloning to assess monoclonality in generating manufacturing cell lines," *Biotechnol. Prog.*, vol. 32, no. 4, pp. 1061–1068, Jul. 2016.

[17] P. A. Underwood and P. A. Bean, "Hazards of the limiting-dilution method of cloning hybridomas," *J. Immunol. Methods*, vol. 107, no. 1, pp. 119–128, Feb. 1988.

[18] A. Traube and T. Brode, *Vorrichtung zur Aufnahme Einer Flüssigkeit Sowie Vorrichtung zur Aufbringung von Flüssigkeiten auf Probenträger und Verfahren Hierzu*, document DE 10 2007 041 071 B4, 2000.

[19] *Dispendix GmbH, Our I-DOT Technology*. Accessed: Dec. 11, 2018. [Online]. Available: http://www.dispendix.com/technology/

[20] L. Schober *et al.*, "Cell dispensing in low-volume range with the immediate drop-on-demand technology (I-DOT)," *J. Lab. Automat.*, vol. 20, no. 2, pp. 154–163, Apr. 2015.

[21] T. Lindemann, "Droplet generation from the nanoliter to the femtoliter range," Ph.D. dissertation, Institut für Mikrosystemtechnik, Univ. Freiburg, Breisgau, Germany, 2006.

[22] O. Gutmann, "Production of custom microarrays using a highly parallel pressure driven nanoliter dispenser," Ph.D. dissertation, Institut für Mikrosystemtechnik, Univ. Freiburg, Breisgau, Germany, 2006.

[23] S. Kroll, "Single cell applications with the immediate drop on demand technology (I-DOT)," M.S. thesis, Institut für Experimentelle Chirurgie, Universität Tübingen, Tübingen, Bingen am Rhein, Germany, 2017.

[24] J. Holz-Müller, "Etablierung eines Verfahrens zur Einzelzelldetektion," M.S. thesis, Institut für Zellbiologie Immunologie, Univ. Stuttgart, Stuttgart, Germany, 2018.

[25] R. Sjöback, J. Nygren, and M. Kubista, "Absorbtion and fluorescence properties of fluorescein," *Spectromica Acta*, vol. 51, pp. 7–21, Jun. 1995.

[26] Polysciences Inc. (2018). *Fluoresbrite Microparticles: Technical Data Sheet 431*. Accessed: Mar. 14, 2019. [Online]. Available: https://www.polysciences.com/skin/frontend/default/polysciences/pdf/TDS%20431.pdf